THEORY

A. AYALA,[1,2] M. HENTSCHINSKI,[3] L.A. HERNÁNDEZ,[1] M. LOEWE,[4,2,5]
R. ZAMORA[6]

[1] Instituto de Ciencias Nucleares, Universidad Nacional Autónoma de México
 (Apartado Postal 70-543, CdMx 04510, Mexico)
[2] Centre for Theoretical and Mathematical Physics, and Department of Physics,
 University of Cape Town
 (Rondebosch 7700, South Africa)
[3] Departamento de Actuaría, Física y Matemáticas, Universidad de las Américas Puebla
 (Santa Catarina Mártir, San Andrés Cholula, 72820 Puebla, Mexico)
[4] Instituto de Física, Pontificia Universidad Católica de Chile
 (Casilla 306, Santiago 22, Chile)
[5] Centro Científico-Tecnológico de Valparaíso CCTVAL,
 Universidad Técnica Federico Santa María
 (Casilla 110-V, Valaparaíso, Chile)
[6] Instituto de Ciencias Básicas, Universidad Diego Portales
 (Casilla 298-V, Santiago, Chile)

EFFECTS OF SUPERSTATISTICS ON THE LOCATION OF THE EFFECTIVE QCD CRITICAL END POINT

Effects of the partial thermalization during the chiral symmetry restoration at the finite temperature and quark chemical potential are considered for the position of the critical end point in an effective description of the QCD phase diagram. We find that these effects cause the critical end point to be displaced toward larger values of the temperature and lower values of the quark chemical potential, as compared to the case where the system can be regarded as completely thermalized. These effects may be important for relativistic heavy ion collisions, where the number of subsystems making up the whole interaction volume can be linked to the finite number of participants in the reaction.

K e y w o r d s: superstatistics, QCD phase diagram, critical end point, relativistic heavy-ion collisions.

The usual thermal description of a relativistic heavy-ion collision assumes that the produced matter reaches equilibrium, characterized by values of the temperature T and the baryon chemical potential μ, common within the whole interaction volume, after some time from the beginning of the reaction. The system evolution is subsequently described by the time evolution of the temperature down to a kinetic freeze-out, where particle spectra are established. This implicitly assumes the validity of the Gibbs–Boltzmann statistics and system's adiabatic evolution.

For expansion rates not too large compared to the interaction rate, the adiabatic evolution can perhaps be safely assumed. However, the Gibbs–Boltzmann statistics can be applied only to systems in the thermodynamical limit, namely, long after the relaxation time has elapsed and the randomization has been achieved within system's volume. In the case of a rela-

tivistic heavy-ion collision, the reaction starts off from nucleon-nucleon interactions. This means that the entire reaction volume is made, at the beginning, of a superposition of interacting pairs of nucleons. If the thermalization is achieved, it seems natural to assume that it starts off in each of the interacting nucleon pair subsystems and later spreads to the entire volume. In this scenario, the temperature and chemical potential within each subsystem may not be the same for other subsystems. Thus, a superposition of statistics, one in the usual Gibbs–Boltzmann sense for particles in each subsystem and another one, for the probability to find particular values for T and μ for different subsystem, seems appropriate. This is described by the so-called superstatistics scenario which describes a nonextensive behavior that naturally arises due to fluctuations in T or μ over the system's volume. This feature could be of particular relevance, when studying the position of the critical end point (CEP) in the QCD phase diagram, where one resorts to measuring ratios of fluctuations in conserved charges with the expectation that the volume factor cancels out in the ratio. If the thermalization is not complete, this expectation cannot hold, and a more sophisticated treatment is called for.

From the theoretical side, efforts to locate the CEP employing several techniques [1–20] were recently carried out. In all of these cases, the full thermalization over the whole reaction volume has been assumed. From the experimental side, the STAR BES-I program has recently studied heavy-ion collisions in the energy range 200 GeV $> \sqrt{s_{NN}} > 7.7$ GeV [21]. Future experiments [22–24] will continue to thoroughly explore the QCD phase diagram, using different system sizes and varying the temperature and baryon density using different collision energies down to about $\sqrt{s_{NN}} \simeq 5$ GeV.

The superstatistics scenario has been explored in the context of relativistic heavy-ion collisions in many papers, *e.g.* Refs. [25–41] and references therein, with a particular focus on the study of imprints of the superstatistics on the particle production, using a particular version, the so-called Tsallis statistics [42]. Its use in the context of the computation of the rapidity distribution profile for the stopping in heavy ion collisions has been recently questioned in Ref. [43]. It has also been implemented to study generalized entropies and generalized Newton's law in Refs. [44–47]. The superstatistics concept has been nicely described in

Refs. [48, 49]. In this work, we summarize the findings of Ref. [50] describing the implications of the superstatistics, when applied to temperature fluctuations for the location of the CEP in the QCD phase diagram.

For a system that has not yet reached a full equilibrium and contains space-time fluctuations of an intensive parameter β, such as the inverse temperature or chemical potential, one can still think of dividing the full volume into spatial subsystems, where β is approximately constant. Within each subsystem, one can apply the ordinary Gibbs–Boltzmann statistics, namely, one can use the ordinary density matrix giving rise to the Boltzmann factor $e^{-\beta \hat{H}}$, where $\hat{H}$ corresponds to the Hamiltonian for the states in each subsystem. The whole system can thus be described in terms of a space-time average over the different values that β could take for the different subsystems. In this way, one obtains a superposition of two statistics, one referring to the Boltzmann factor $e^{-\beta \hat{H}}$ and the other for β, hence, the name superstatistics.

To implement the scenario, one defines an averaged Boltzmann factor

$$B(\hat{H}) = \int_0^\infty f(\beta) e^{-\beta \hat{H}} d\beta, \qquad (1)$$

where $f(\beta)$ is the probability distribution of β. The partition function then becomes

$$Z = \text{Tr}[B(\hat{H})] = \int_0^\infty B(E) dE, \qquad (2)$$

where the last equality holds for a suitably chosen set of eigenstates of the Hamiltonian.

When all the subsystems can be described with the same probability distribution [44], a possible choice to distribute the random variable β is the χ^2 distribution,

$$f(\beta) = \frac{1}{\Gamma(N/2)} \left(\frac{N}{2\beta_0}\right)^{N/2} \beta^{N/2-1} e^{-N\beta/2\beta_0}, \qquad (3)$$

where Γ is the Gamma function, N represents the number of subsystems that make up the whole system, and

$$\beta_0 \equiv \int_0^\infty \beta f(\beta) d\beta = \langle \beta \rangle \qquad (4)$$

is the average of the distribution. The χ^2 is the distribution that emerges for a random variable that is made up of the sum of the squares of random variables X_i, each of which is distributed with a Gaussian probability distribution with vanishing average and unit variance. This means that if we take

$$\beta = \sum_{i=1}^{N} X_i^2, \tag{5}$$

then β is distributed according to Eq. (3). Moreover, its variance is given by

$$\langle \beta^2 \rangle - \beta_0^2 = \frac{2}{N} \beta_0^2. \tag{6}$$

Given that β is a positive definite quantity, thinking of it as being the sum of positive definite random variables is an adequate model. Note, however, that these variables do not necessarily correspond to the inverse temperature in each of the subsystems. Nevertheless, since the use of the χ^2 distribution allows for an analytical treatment, we hereby take this as the distribution to model the possible values of β.

To add superstatistics effects to the dynamics of a given system, we first find the effective Boltzmann factor. This is achieved by taking Eq. (3) and substituting it into Eq. (1). The integration over β leads to

$$B(\hat{H}) = \left(1 + \frac{2}{N} \beta_0 \hat{H}\right)^{-\frac{N}{2}}. \tag{7}$$

Note that, in the limit as $N \to \infty$, Eq. (7) becomes the ordinary Boltzmann factor. For large, but finite N, Eq. (7) can be expanded as

$$B(\hat{H}) = \left[1 + \frac{1}{2}\left(\frac{2}{N}\right)\beta_0^2 \hat{H}^2 - \frac{1}{3}\left(\frac{2}{N}\right)^2 \beta_0^3 \hat{H}^3 + ...\right] e^{-\beta_0 \hat{H}}. \tag{8}$$

Working up to first order in $1/N$, Eq. (8) can be written as [48]

$$B(\hat{H}) = e^{-\beta \hat{H}} \left(1 + \frac{\beta^2 H^2}{N} + ...\right) =$$
$$= \left[1 + \frac{\beta_0^2}{N} \left(\frac{\partial}{\partial \beta_0}\right)^2 + ...\right] e^{-\beta_0 \hat{H}}. \tag{9}$$

Therefore, the partition function to the first order in $1/N$ is given by

$$Z = \left[1 + \frac{\beta_0^2}{N} \left(\frac{\partial}{\partial \beta_0}\right)^2 + ...\right] Z_0 \tag{10}$$

with

$$Z_0 = e^{-\mathtt{V}\beta_0 V^{\text{eff}}}, \tag{11}$$

where $\mathtt{V}$ and V^{eff} are the system's volume and effective potential, respectively. After a bit of a straightforward algebra, we write the expression for the partition function in terms of $T_0 = 1/\beta_0$ as

$$Z = \left[1 + \frac{\beta_0^2}{N} \left(\frac{\partial}{\partial \beta_0}\right)^2 + ...\right] Z_0 =$$
$$= Z_0 \left[1 + \frac{2T_0}{NZ_0} \left(\frac{\partial Z_0}{\partial T_0} + \frac{T_0}{2} \frac{\partial^2 Z_0}{\partial T_0^2}\right)\right], \tag{12}$$

and, therefore,

$$\ln[Z] = \ln[Z_0] + \ln\left[1 + \frac{2T_0}{NZ_0} \left(\frac{\partial Z_0}{\partial T_0} + \frac{T_0}{2} \frac{\partial^2 Z_0}{\partial T_0^2}\right)\right]. \tag{13}$$

To explore the QCD phase diagram from the point of view of chiral symmetry restoration, we use an effective model that accounts for the physics of spontaneous symmetry breaking at finite temperature and density: the linear sigma model. In order to account for the fermion degrees of freedom around the phase transition, we also include quarks in this model and work with the linear sigma model with quarks. The Lagrangian in the case where only the two lightest quark flavors are included is given by

$$\mathcal{L} = \frac{1}{2}(\partial_\mu \sigma)^2 + \frac{1}{2}(\partial_\mu \boldsymbol{\pi})^2 + \frac{a^2}{2}(\sigma^2 + \boldsymbol{\pi}^2) +$$
$$+ \frac{\lambda}{4}(\sigma^2 + \boldsymbol{\pi}^2)^2 + i\bar{\psi}\gamma^\mu \partial_\mu \psi - g\bar{\psi}(\sigma + i\gamma_5 \boldsymbol{\tau} \, \boldsymbol{\pi})\psi, \tag{14}$$

where ψ is an SU(2) isospin doublet, $\boldsymbol{\pi} = (\pi_1, \pi_2, \pi_3)$ is an isospin triplet, σ is an isospin singlet, λ is the boson's self-coupling, g is the fermion-boson coupling, and $a^2 > 0$ is the squared mass parameter.

To allow for an spontaneous symmetry breaking, we let the σ field develop a vacuum expectation value v

$$\sigma \to \sigma + v, \tag{15}$$

which serves as the order parameter to identify the phase transitions. After this shift, the Lagrangian can be rewritten as

$$\mathcal{L} = \frac{1}{2}(\partial_\mu \sigma)^2 - \frac{1}{2}\left(3\lambda v^2 - a^2\right)\sigma^2 +$$

$$+ \frac{1}{2}(\partial_\mu \boldsymbol{\pi})^2 - \frac{1}{2}\left(\lambda v^2 - a^2\right)\boldsymbol{\pi}^2 + \frac{a^2}{2}v^2 +$$

$$-\frac{\lambda}{4}v^4 + i\bar{\psi}\gamma^\mu \partial_\mu \psi - gv\bar{\psi}\psi + \mathcal{L}_I^b + \mathcal{L}_I^f, \tag{16}$$

where the sigma, three pions, and the quarks have masses given by

$$\begin{aligned} m_\sigma^2 &= 3\lambda v^2 - a^2, \\ m_\pi^2 &= \lambda v^2 - a^2, \\ m_f &= gv, \end{aligned} \tag{17}$$

respectively, and $\mathcal{L}_I^b$ and $\mathcal{L}_I^f$ are given by

$$\begin{aligned} \mathcal{L}_I^b &= -\frac{\lambda}{4}(\sigma^2 + \boldsymbol{\pi}^2)^2 \\ \mathcal{L}_I^f &= -g\bar{\psi}(\sigma + i\gamma_5 \boldsymbol{\tau} \cdot \boldsymbol{\pi})\psi. \end{aligned} \tag{18}$$

Equation (18) describes the interactions among the σ, $\boldsymbol{\pi}$, and ψ fields after the symmetry breaking.

In order to analyze the chiral symmetry restoration, we compute the effective potential at finite temperature and density. In order to account for plasma screening effects, we also work up to the contribution of ring diagrams. All matter terms are computed in the high-temperature approximation. The effective potential is given by [20]

$$V^{\mathrm{eff}}(v, T_0, \mu_q) = -\frac{(a^2 + \delta a^2)}{2}v^2 + \frac{(\lambda + \delta\lambda)}{4}v^4 +$$

$$+ \sum_{b=\sigma,\bar{\pi}} \left\{ -\frac{m_b^4}{64\pi^2}\left[\ln\left(\frac{a^2}{4\pi T_0^2}\right) - \gamma_E + \frac{1}{2}\right] - \right.$$

$$\left. -\frac{\pi^2 T_0^4}{90} + \frac{m_b^2 T_0^2}{24} - \frac{(m_b^2 + \Pi(T_0, \mu_q))^{3/2}T_0}{12\pi} \right\} +$$

$$+ \sum_{f=u,d} \left\{ \frac{m_f^4}{16\pi^2}\left[\ln\left(\frac{a^2}{4\pi T_0^2}\right) - \gamma_E + \frac{1}{2} - \right.\right.$$

$$\left. -\psi^0\left(\frac{1}{2} + \frac{\mathrm{i}\mu_q}{2\pi T_0}\right) - \psi^0\left(\frac{1}{2} - \frac{\mathrm{i}\mu_q}{2\pi T_0}\right)\right] -$$

$$-8m_f^2 T_0^2\left[\mathrm{Li}_2(-e^{\mu_q/T_0}) + \mathrm{Li}_2(-e^{-\mu_q/T_0})\right] +$$

$$\left. + 32T_0^4\left[\mathrm{Li}_4(-e^{\mu_q/T_0}) + \mathrm{Li}_4(-e^{-\mu_q/T_0})\right]\right\}, \tag{19}$$

where μ_q is the quark chemical potential, and δa^2 and $\delta\lambda$ represent the counterterms which ensure that

the one-loop vacuum corrections do not shift the position of the minimum or the vacuum mass of the sigma. These counterterms are given by

$$\begin{aligned} \delta a^2 &= -a^2 \frac{(8g^4 - 12\lambda^2 - 3\lambda^2 \ln[2])}{32\pi\lambda}, \\ \delta\lambda &= \frac{(16 + 8\ln[g^2/\lambda])g^4 - (18 + 9\ln[2])\lambda^2}{64\pi^2}. \end{aligned} \tag{20}$$

The self-energy at finite temperature and quark chemical potential, $\Pi(T_0, \mu_q)$, includes the contribution from both bosons and fermions. In the high temperature approximation, it is given by [20]

$$\Pi(T_0, \mu_q) = -N_f N_c g^2 \frac{T_0^2}{\pi^2}\Big[\mathrm{Li}_2(-e^{\mu_q/T_0}) +$$

$$+ \mathrm{Li}_2(-e^{-\mu_q/T_0})\Big] + \frac{\lambda T_0^2}{2}. \tag{21}$$

To implement superstatistics corrections, we substitute Eq. (19) into Eq. (11). The partition function is obtained from Eq. (12) and the effective potential including superstatistics effects is obtained from the logarithm of this partition function,

$$V_{\mathrm{sup}}^{\mathrm{eff}} = -\frac{1}{\mathsf{V}\beta}\ln[Z]. \tag{22}$$

As a consequence, the effective potential of Eq. (22) has four free parameters. Three of them come from the original model, namely, λ, g and a. The remaining one corresponds to the superstatistics correction, N. In the absence of superstatistics, the effective potential in Eq. (19) allows for the second- and first-order phase transitions, depending on the values of λ, g and a, as well as of T_0 and μ_q. For given values of λ, g, and a, we now proceed to analyze the phase structure that emerges, when varying N, paying particular attention to the displacement of the CEP location in the T_0, μ_q plane.

The figure shows the effective QCD phase diagram calculated with $a = 133$ MeV, $g = 0.51$, and $\lambda = 0.36$ for different values of the number of subsystems making up the whole system, N. For the different curves, the star shows the position of the CEP. Note that this position moves to larger values of T and lower values of μ_q, with respect to the CEP position for $N = \infty$, that is, without superstatistics effects, as N decreases. Note also that, for these findings, we have not considered fluctuations in the chemical potential. Those have been included to study the CEP position in the Nambu–Jona-Lasinio model in Ref. [53].

Our findings show that fermions become more relevant for lower values of the baryon chemical potential, than they do in the case of the homogeneous system. To picture this result, as above, let (μ_c^0, T_c^0) and (μ_c, T_c) be the critical values for the baryon chemical potential and temperature at the onset of first-order phase transitions for the homogeneous and fluctuating systems, respectively. The parameter that determines, when fermions become relevant, is the combination μ_c^0/T_c^0. Since our calculation for a single-boson degrees of freedom shows that the critical temperature decreases with decreasing the number of subsystems (see Ref. [50]), this means that, for the boson-fermion fluctuating system, fermions become relevant for $\mu_c/T_c \simeq \mu_c^0/T_c^0$ and, thus, for $\mu_c < \mu_c^0$.

To apply these considerations to the context of relativistic heavy-ion collisions, we recall that temperature fluctuations are related to the system's heat capacity by

$$\frac{(1-\xi)}{C_v} = \frac{\langle (T - T_0)^2 \rangle}{T_0^2}, \qquad (23)$$

where the factor $(1 - \xi)$ accounts for deviations [54] from the Gaussian [55] distribution for the random variable T. The right-hand side of Eq. (23) can be written in terms of fluctuations in β as

$$\frac{\langle (T - T_0)^2 \rangle}{T_0^2} \frac{\langle T^2 \rangle - T_0^2}{T_0^2} = \frac{\beta_0^2 - \langle \beta^2 \rangle}{\langle \beta^2 \rangle} =$$
$$= \frac{\left(\frac{\beta_0^2}{\langle \beta^2 \rangle} \right)^2 \langle \beta^2 \rangle - \beta_0^2}{\beta_0^2}. \qquad (24)$$

Note that, according to Eq. (6),

$$\left(\frac{\beta_0^2}{\langle \beta^2 \rangle} \right)^2 = \left(\frac{1}{1 + 2/N} \right)^2 \simeq 1 - 4/N. \qquad (25)$$
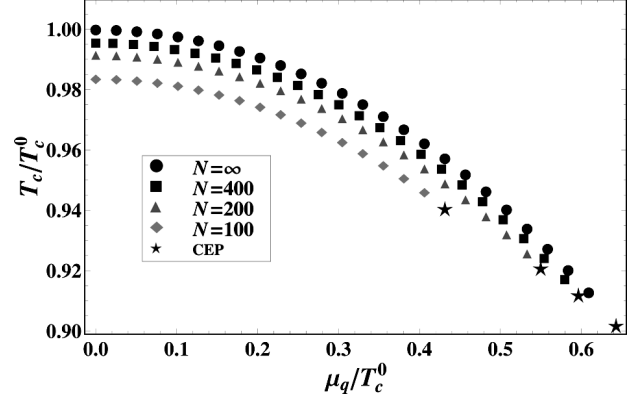
Therefore, for N finite, but large,

$$\frac{\langle (T - T_0)^2 \rangle}{T_0^2} \simeq \frac{\langle \beta^2 \rangle - \beta_0^2}{\beta_0^2}. \qquad (26)$$

Using Eqs. (6) and (26), we obtain

$$\frac{\langle (T - T_0)^2 \rangle}{T_0^2} = \frac{2}{N}. \qquad (27)$$

This means that the heat capacity is related to the number of subsystems by

$$\frac{(1-\xi)}{C_v} = \frac{2}{N}. \qquad (28)$$

Effective QCD phase diagram calculated with $a = 133$ MeV, $g = 0.51$, and $\lambda = 0.36$ for different values of N. The star shows the position of the CEP which moves toward larger values of T and lower values of μ_q, as N decreases

To introduce the specific heat c_v for a relativistic heavy-ion collision, it is natural to divide C_v by the number of participants N_p in the reaction. Therefore, Eq. (28) can be written as

$$\frac{2}{N} = \frac{(1-\xi)}{N_p c_v}. \qquad (29)$$

In Ref. [54], ξ is estimated as $\xi = N_p/A$, where A is the smallest mass number of the colliding nuclei. Equation (29) provides the link between the number of subsystems in a general superstatistics framework and a relativistic heavy-ion collision. It has been shown [56] that, at least for Gaussian fluctuations, c_v is a function of the collision energy. Therefore, in order to make a thorough exploration of the phase diagram, as the collision energy changes, we need to account for this dependence, as well as to work with values of the model parameters λ, g, and a, appropriate to the description of the QCD phase transition. Work along these lines is currently underway and will be reported elsewhere.

1. A. Ayala, C. A. Dominguez, M. Loewe. For a recent review on the QCD sum rules technique at finite temperature. *Adv. High Energy Phys.* **2017**, 9291623 (2017).

2. P. Costa, M.C. Ruivo, C.A. de Sousa. Thermodynamics and critical behavior in the Nambu–Jona-Lasinio model of QCD. *Phys. Rev. D* **77**, 096001 (2008).

3. G.A. Contrera, D. Gomez-Dumm, N.N. Scoccola. Nonlocal SU(3) chiral quark models at finite temperature: The role of the Polyakov loop. *Phys. Lett. B* **661**, 113 (2008).

4. A. Ayala, A. Bashir, C. A. Dominguez, E. Gutierrez, M. Loewe, A. Raya. QCD phase diagram from finite energy sum rules. *Phys. Rev. D* **84**, 056004 (2011).

5. X.-Y. Xin, S.-X. Qin, Y.-X. Liu. Quark number fluctuations at finite temperature and finite chemical potential via the Dyson–Schwinger equation approach. *Phys. Rev. D* **90**, 076006 (2014).

6. C.S. Fischer, J. Luecker, C.A. Welzbacher. Phase structure of three and four flavor QCD. *Phys. Rev. D* **90**, 034022 (2014).

7. Y. Lu, Y.-L. Du, Z.-F. Cui, H.-S. Zong. Critical behaviors near the (tri-) critical end point of QCD within the NJL model. *Eur. Phys. J. C* **75**, 495 (2015).

8. A. Ayala, M. Loewe, R. Zamora. Inverse magnetic catalysis in the linear sigma model with quarks. *Phys. Rev. D* **91**, 016002 (2015).

9. A. Ayala, M. Loewe, A.J. Mizher, R. Zamora. Inverse magnetic catalysis for the chiral transition induced by thermomagnetic effects on the coupling constant. *Phys. Rev. D* **90**, 036001 (2014).

10. A. Ayala, C.A. Dominguez, L.A. Hernández, M. Loewe, R. Zamora. Magnetized effective QCD phase diagram. *Phys. Rev. D* **92**, 096011 (2015).

11. C. Shi, Y.-L. Du, S.-S. Xu, X.-J. Liu, H.-S. Zong. Continuum study of the QCD phase diagram through an OPE-modified gluon propagator. *Phys. Rev. D* **93**, 036006 (2016).

12. G.A. Contrera, A.G. Grunfeld, D. Blaschke. Supporting the search for the CEP location with nonlocal PNJL models constrained by lattice QCD. *Eur. Phys. J. A* **52**, 231 (2016).

13. A. Ayala, C.A. Dominguez, L.A. Hernández, M. Loewe, A. Raya, J.C. Rojas, C. Villavicencio. Thermomagnetic properties of the strong coupling in the local Nambu–Jona-Lasinio model. *Phys. Rev. D* **94**, 054019 (2016).

14. Z.-F. Cui, J.-L. Zhang, H.-S. Zong. Proper time regularization and the QCD chiral phase transition. *Sci. Rep.* **7**, 45937 (2017).

15. S. Datta, R.V. Gavai, S. Gupta. Quark number susceptibilities and equation of state at finite chemical potential in staggered QCD with $N_t = 8$. *Phys. Rev. D* **95**, 054512 (2017).

16. J.P. Carlomagno, M. Loewe. Comparison between the continuum threshold and the Polyakov loop as deconfinement order parameters. *Phys. Rev. D* **95**, 036003 (2017).

17. J. Knaute, R. Yaresko, B. Kämpfer. Holographic QCD phase diagram with critical point from Einstein–Maxwell-dilaton dynamics. *Phys. Lett. B* **778**, 419 (2018).

18. N.G. Antoniou, F.K. Diakonos, X.N. Maintas. C.E. Tsagkarakis. Locating the QCD critical endpoint through finite-size scaling. *Phys. Rev. D* **97**, 034015 (2018).

19. R. Rougemont, R. Critelli, J. Noronha-Hostler, J. Noronha, C. Ratti. Dynamical versus equilibrium properties of the QCD phase transition: A holographic perspective. *Phys. Rev. D* **96**, 014032 (2017).

20. A. Ayala, S. Hernández-Ortiz, L.A. Hernández. QCD phase diagram from chiral symmetry restoration: analytic approach at high and low temperature using the linear sigma model with quarks. *Rev. Mex. Fis.* **64**, 302 (2018).

21. L. Adamczyk *et al.*, [STAR Collaboration]. Energy dependence of moments of net-proton multiplicity distributions at RHIC. *Phys. Rev. Lett.* **112**, 032302 (2014); Beam energy dependence of moments of the net-charge multiplicity distributions in Au + Au collisions at RHIC. *Phys. Rev. Lett.* **113**, 092301 (2014).

22. C. Yang, [for the STAR Collaboration]. The STAR beam energy scan phase II physics and upgrades. *Nucl. Phys. A* **967**, 800 (2017).

23. P. Senger. The heavy-ion program of the future FAIR facility. *J. Phys. Conf. Ser.* **798**, 012062 (2017).

24. V. Kekelidze, A. Kovalenko, R. Lednicky, V. Matveev, I. Meshkov, A. Sorin, G. Trubnikov. Feasibility study of heavy-ion collision physics at NICA JINR. *Nucl. Phys. A* **967**, 884 (2017).

25. G. Wilk, Z. Wlodarczyk. Multiplicity fluctuations due to the temperature fluctuations in high-energy nuclear collisions. *Phys. Rev. C* **79**, 054903 (2009).

26. G. Wilk, Z. Wlodarczyk. Power laws in elementary and heavy-ion collisions. *Eur. Phys. J. A* **40**, 299 (2009).

27. G. Wilk, Z. Wlodarczyk. The imprints of superstatistics in multiparticle production processes. *Cent. Eur. J. Phys.* **10**, 568 (2012).

28. M. Rybczynski, Z. Wlodarczyk. Tsallis statistics approach to the transverse momentum distributions in p-p collisions. *Eur. Phys. J. C* **74**, 2785 (2014).

29. C.Y. Wong, G. Wilk, L.J.L. Cirto, C. Tsallis. From QCD-based hard-scattering to nonextensive statistical mechanical descriptions of transverse momentum spectra in high-energy pp and $p\bar{p}$ collisions. *Phys. Rev. D* **91**, 114027 (2015).

30. G. Wilk, Z. Wlodarczyk. Superstatistical cluster decay. *Phys. Lett. A* **379**, 2941 (2015).

31. A. Bialas. Tsallis $p_\perp$ distribution from statistical clusters. *Phys. Lett. B* **747**, 190 (2015).

32. T. Bhattacharyya, J. Cleymans, A. Khuntia, P. Pareek, R. Sahoo. Radial flow in non-extensive thermodynamics

and study of particle spectra at LHC in the limit of small $(q-1)$. *Eur. Phys. J. A* **52**, 30 (2016).

33. A. Bialas, A. Bzdak. Short-range two-particle correlations from statistical clusters. *Phys. Rev. D* **93**, 094015 (2016).

34. J. Rozynek, G. Wilk. An example of the interplay of nonextensivity and dynamics in the description of QCD matter. *Eur. Phys. J. A* **52**, 294 (2016).

35. S. Tripathy, T. Bhattacharyya, P. Garg, P. Kumar, R. Sahoo, J. Cleymans. Nuclear modification factor using Tsallis non-extensive statistics. *Eur. Phys. J. A* **52**, 289 (2016).

36. S. Grigoryan. Using the Tsallis distribution for hadron spectra in *pp* collisions: Pions and quarkonia at $\sqrt{s} = 5$–13000 GeV. *Phys. Rev. D* **95**, 056021 (2017).

37. A. Khuntia, S. Tripathy, R. Sahoo, J. Cleymans. Multiplicity dependence of non-extensive parameters for strange and multi-strange particles in proton-proton collisions at $\sqrt{s} = 7$ TeV at the LHC. *Eur. Phys. J. A* **53**, 103 (2017).

38. T. Bhattacharyya, J. Cleymans, L. Marques, S. Mogliacci, M.W. Paradza. On the precise determination of the Tsallis parameters in proton-proton collisions at LHC energies. *J. Phys. G* **45**, 055001 (2018).

39. S. Tripathy, S.K. Tiwari, M. Younus, R. Sahoo. Elliptic flow in Pb+Pb collisions at $\sqrt{s_{\mathrm{NN}}} = 2.76$ TeV at the LHC using Boltzmann transport equation with non-extensive statistics. *Eur. Phys. J. A* **54**, 38 (2018).

40. M. Ishihara. Phase transition for the system of finite volume in the ϕ^4 theory in the Tsallis nonextensive statistics. *Int. J. Mod. Phys. A* **33**, 1850067 (2018).

41. G. Wilk, Z. Wlodarczyk. Some intriguing aspects of multiparticle production processes. *Int. J. Mod. Phys. A* **33**, 1830008 (2018).

42. C. Tsallis. Possible generalization of Boltzmann–Gibbs statistics. *J. Stat. Phys.* **52**, 479 (1988).

43. A. Simon, G. Wolschin. Examining nonextensive statistics in relativistic heavy-ion collisions. *Phys. Rev. C* **97**, 044913 (2018).

44. O. Obregón, A. Gil-Villegas. Generalized information entropies depending only on the probability distribution. *Phys. Rev. E* **88**, 062146 (2013).

45. A. Martínez-Merino, O. Obregón, M.P. Ryan, jr. Modified entropies, their corresponding Newtonian forces, potentials, and temperatures. *Phys. Rev. D* **95**, 124031 (2017).

46. O. Obregón. Superstatistics and gravitation. *Entropy 2010* **12**, 2067 (2010).

47. O. Obregón. Superstatistics and gravitation. *Entropy 2010* **12**, 2067 (2010).

48. C. Beck, E.G.D. Cohen. Superstatistics. *Phys. A* **322**, 267 (2003).

49. C. Beck. Superstatistics: theory and applications. *Continuum Mech. Thermodyn.* **16**, 293 (2004); C. Beck. Recent developments in superstatistics. *Braz. J. Phys.* **39**, 2A, 357 (2009).

50. Al. Ayala, M. Hentschinski, L.A. Hernandez, M. Loewe, R. Zamora. Superstatistics and the effective QCD phase diagram. *Phys. Rev. D* **98**, 114002 (2018).

51. A. Ayala, A. Sanchez, G. Piccinelli, S. Sahu. Effective potential at finite temperature in a constant magnetic field. I. Ring diagrams in a scalar theory. *Phys. Rev. D* **71**, 023004 (2005).

52. M.E. Carrington. The effective potential at finite temperature in the Standard Model. *Phys. Rev. D* **45**, 2933 (1992).

53. J. Rozynek, G. Wilk. An example of the interplay of nonextensivity and dynamics in the description of QCD matter. *Eur. Phys. J. A* **52**, 294 (2016).

54. G. Wilk, Z. Wlodarczyk. Multiplicity fluctuations due to the temperature fluctuations in high-energy nuclear collisions. *Phys. Rev. C* **79**, 054903 (2009).

55. L.D. Landau, E.M. Lifshitz. *Statistical Physics* (Elsevier, 2013), ISBN 9780080570464.

56. S. Basu, S. Chatterjee, R. Chatterjee, T.K. Nayak, B.K. Nandi. Specific heat of matter formed in relativistic nuclear collisions. *Phys. Rev. C* **94**, 044901 (2016).

А. Аяла, М. Хентшинскі,
Л.А. Гернандез, М. Леве, Р. Замора

ВПЛИВ СУПЕРСТАТИСТИКИ
НА ПОЛОЖЕННЯ КРИТИЧНОЇ КІНЦЕВОЇ
ТОЧКИ В ЕФЕКТИВНІЙ КХД

Р е з ю м е

В рамках ефективної моделі фазової діаграми КХД розглядається вплив часткової термалізації під час відновлення кіральної симетрії при скінченних температурі і хімічному потенціалі кварків на положення критичної кінцевої точки. Ми показали, що ці ефекти спричиняють зміщення критичної точки в бік більших температур та менших значень хімічного потенціалу кварків по відношенню до повністю термалізованої системи. Ці ефекти можуть бути важливими для зіткнень релятивістських важких іонів, де число підсистем, що заповнюють весь об'єм, можна пов'язати зі скінченним числом частинок в реакції.